

Reconfigurable Intelligent Surface-Empowered MIMO Systems

Aymen Khaleel, *Student Member, IEEE* and Ertugrul Basar, *Senior Member, IEEE*

Abstract—Reconfigurable intelligent surface (RIS)-assisted communications appear as a promising candidate for future wireless systems due to its attractive advantages in terms of implementation cost and end-to-end system performance. In this paper, two new multiple-input multiple-output (MIMO) system designs using RISs are presented to enhance the performance and boost the spectral efficiency of state-of-the-art MIMO communication systems. Vertical Bell Labs layered space-time (VBLAST) and Alamouti's schemes have been considered in this study and RIS-based simple transceiver architectures are proposed. For the VBLAST-based new system, an RIS is used to enhance the performance of the nulling and canceling-based sub-optimal detection procedure as well as to noticeably boost the spectral efficiency by conveying extra bits through the adjustment of the phases of the RIS elements. In addition, RIS elements have been utilized in order to redesign Alamouti's scheme with a single radio frequency (RF) signal generator at the transmitter side and to enhance its bit error rate (BER) performance. Monte Carlo simulations are provided to show the effectiveness of our system designs and it has been shown that they outperform the reference schemes in terms of BER performance and spectral efficiency.

Index Terms—Reconfigurable intelligent surface (RIS), MIMO systems, error probability analysis, VBLAST, Alamouti's scheme.

I. INTRODUCTION

RECONFIGURABLE intelligent surfaces (RISs) have received significant attention from the wireless communication community as effective, cheap, reconfigurable, easy to deploy, and passive system modules that can be used to control the wireless propagation environment by re-engineering the electromagnetic waves [1], [2]. Manipulating the propagation environment using RISs has been regarded as a promising candidate for the next-generation wireless technologies such as Terahertz communications, non-orthogonal multiple access (NOMA), and low-cost massive multiple-input multiple-output (MIMO) systems. Without loss of generality, mitigating the fading channel impairments and compensating for the propagation losses in order to enhance the signal quality at the receiver side are the main objectives behind the development of this technology. Nevertheless, RISs can also be utilized to minimize the transmitted signal power, to boost the system transmission capacity, and to enhance the physical layer security [3], [4].

In the preliminary study of [5], RISs are employed for two different purposes. First, an RIS is used to realize an ultra-

reliable communication scheme that operates at considerably low signal-to-noise ratio (SNR) values. While in the second scenario, an RIS is used as an access point to create virtual phase shift keying (PSK) symbols at the receiver side. The latter concept is also used to perform index modulation at the receiver side [6]. In [7], the indoor multiple-user network-sharing capacity is enhanced by optimally adjusting the phases of a passive reconfigurable reflect-array to cancel the interference and enhance the users' signal quality. An energy efficient multiple-input single output (MISO) system is proposed in [8], by jointly optimizing the transmit powers of the users and the phases of RIS elements. In [9] and [10], the received signal power for a MISO user is maximized by optimizing the active beamforming at the transmitter jointly with the passive beamforming at the RIS by adjusting its phase shifters. The latter concept is also used in [11], where the beamformer at the access point and RIS are jointly optimized in order to increase the spectral efficiency for an RIS-assisted multi-user MISO system. In [12], an RIS-assisted multi-user MISO system is considered with different channel types where RIS phase optimization is utilized in order to maximize the minimum signal-to-noise-and-interference ratio (SNIR). RIS is used in [13] to improve the channel rank for MIMO systems by adding additional multipaths with distinctively different spatial angles in addition to the low-rank direct channel path. RIS reflection coefficients and the transmit covariance matrix are jointly optimized in [14] in order to maximize the capacity of a point-to-point MIMO system. The latter optimization technique is also used in [15] to increase the secrecy rate for a MIMO multiple eavesdropper scenario where the access point, the legitimate user, and the eavesdropper all equipped with multiple antennas. In [16], the authors consider the channel estimation problem in multi-user MIMO systems and propose an uplink channel estimation protocol to estimate the cascaded channel from the base station to the RIS and from the RIS to the user. However, the use of RISs to boost the spectral efficiency and/or reliability of existing MIMO systems along with applications of index modulation (IM) is not well explored in the open literature.

Against this background, two new RIS-assisted communication schemes are presented in this paper by focusing on the integration of RISs into the existing MIMO systems in a simple and effective way. VBLAST [17] and Alamouti's schemes [18] are considered in this study as the most common and practical MIMO schemes while a generalization to other advanced MIMO signaling schemes might be possible using our concept. First, an RIS-assisted Alamouti's scheme with a single RF signal generator at the transmitter side is presented.

The authors are with the Communications Research and Innovation Laboratory (CoreLab), Department of Electrical and Electronics Engineering, Koç University, Sariyer 34450, Istanbul, Turkey. Email: akhaleel18@ku.edu.tr, ebasar@ku.edu.tr

At the receiver side, the classical Alamouti's detector is used to recover the transmitted symbols, assuming that the channel state information (CSI) is available at this unit. Computer simulation results show a significant performance improvement for the proposed scheme against the blind RIS scheme in [5] and the classical Alamouti's scheme. It is worth noting that, for this scheme, the CSI between the RIS elements and the receiving antenna is not needed at the RIS. Consequently, our scheme appears as a simple implementation method for space-time coding systems that require multiple antennas as well as RF chains.

Second, an RIS-assisted and IM-based VBLAST scheme is introduced using nulling and cancelling-based sub-optimal detection with zero forcing (ZF) technique. Unlike the RIS-assisted Alamouti's scheme, CSI between each transmit-receive antenna pair through the RIS is required in this setup. The RIS can be operated in multiple modes with and without IM. With IM, the RIS eliminates the channel phases between a specific transmit-receive antenna pair, which is selected according to the additional information bits in an IM fashion. At the other hand, without IM, the RIS eliminates the channel phases between a fixed and predefined antenna pair in order to provide the maximum BER performance enhancement. At the receiver side, we propose two novel nulling-based detectors to detect the indices of the antennas targeted by the IM. Furthermore, the transmitted symbols will be detected as in the plain VBLAST scheme using ZF-based nulling and cancelling algorithm without requiring additional signal processing steps at the receiver side [17]. The proposed schemes are simple in design and do not require major modifications for the state-of-the-art systems. Furthermore, comprehensive computer simulations are provided in this study under realistic environment setups to assess their practical feasibility.

The rest of the paper is organized as follows. In Section II, we introduce the system model of the RIS-assisted Alamouti's scheme and evaluate its symbol error probability (SEP). Section III introduces the RIS-assisted and IM-based VBLAST scheme, the nulling-based detectors, and the analysis of the computational complexity of the receiver. In Section IV, we provide our computer simulation results and comparisons along with path loss models considered in these simulations. Finally, conclusions are given in Section V.

II. RIS-ASSISTED ALAMOUTI'S SCHEME: SIGNAL MODEL AND ERROR PERFORMANCE ANALYSIS

In the proposed RIS-assisted Alamouti's scheme, an unmodulated carrier signal is being transmitted from a low-cost RF signal generator close to the source (S) unit. The RF signal generator contains an RF digital-to-analog converter with an internal memory and a power amplifier as discussed in [5]. Fig. 1 shows the block diagram of the proposed scheme where r_s and r_d are the distances (in meters) of S-RIS and RIS-D, respectively. r_s is selected in a way that the channel between S and RIS is assumed to be line-of-sight (LOS) dominated. In our setup, the RIS is divided into two parts each having $N/2$ elements adjusted to a common reflection phase value. Each part employs two

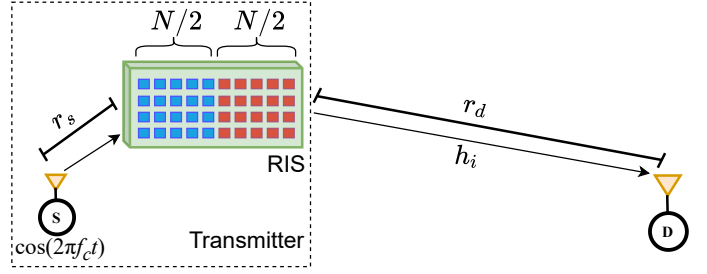


Fig. 1. RIS-assisted Alamouti's scheme with the RIS as the transmitter.

different common reflection phase values over two time slots. The proposed system emulates the Alamouti's scheme by adjusting the phases of the RIS elements to modify the RF carrier signal and invoke the phases of the two data symbols. In this way, the Alamouti's scheme can be redesigned with a single RF signal generator instead of two full RF chains at the transmitter side. The RIS is a blind one with respect to the CSI, while its intelligence stems from the fact that it adjusts the unmodulated RF signal to mimic the PSK symbol phases.

Let h_i denote the small-scale fading channel coefficient between the destination (D) and i^{th} element of the RIS, we have $h_i \sim \mathcal{CN}(0, 1)$ under Rayleigh fading assumption, where $\mathcal{CN}(0, \sigma^2)$ stands for complex Gaussian distribution with zero mean and σ^2 variance. θ_0 and θ_1 stand for the phases of two M -PSK symbols to be transmitted according to $2 \log_2(M)$ bits. Assuming quasi-static fading channels, where the channels will remain constant over the two time slots, the received signal at the first time slot can be written as

$$r_0 = \sqrt{P_L} \left[\sqrt{E_s} e^{j\theta_0} \sum_{i=1}^{N/2} h_i + \sqrt{E_s} e^{j\theta_1} \sum_{i=\frac{N}{2}+1}^N h_i \right] + n_0 \quad (1)$$

where n_0 is the additive white Gaussian noise (AWGN) sample at the first time slot, $n_0 \sim \mathcal{CN}(0, N_0)$. E_s is the transmitted RF signal energy and θ_0 and θ_1 are the common RIS reflection phases for the first and second parts, respectively, for the first time slot. P_L is the total path gain (loss), and more details regarding the considered path loss model and environmental setups will be given in Section IV. According to the Alamouti's transmission scheme, in the second time slot, we obtain the following received signal by carefully adjusting the common RIS phase terms as $-(\theta_1 + \pi)$ and $-\theta_0$ for the first and second parts, respectively:

$$r_1 = \sqrt{P_L} \left[\sqrt{E_s} e^{-j(\theta_1 + \pi)} \sum_{i=1}^{N/2} h_i + \sqrt{E_s} e^{-j\theta_0} \sum_{j=\frac{N}{2}+1}^N h_j \right] + n_1 \quad (2)$$

where $n_1 \sim \mathcal{CN}(0, N_0)$. Defining $s_0 = \sqrt{E_s} e^{\theta_0}$, $s_1 = \sqrt{E_s} e^{\theta_1}$, $A_0 = \sqrt{P_L} \sum_{i=1}^{N/2} h_i$ and $A_1 = \sqrt{P_L} \sum_{i=\frac{N}{2}+1}^N h_i$, (1) and (2) can be re-expressed as

$$r_0 = s_0 A_0 + s_1 A_1 + n_0 \quad (3)$$

$$r_1 = -s_1^* A_0 + s_0^* A_1 + n_1 \quad (4)$$

where s_0 and s_1 stand for two virtual M -PSK symbols to be delivered to the receiver and M is the modulation order. As in the classical Alamouti's scheme, the combiner will construct

the combined signals as follows:

$$\tilde{s}_0 = r_0 A_0^* + r_1^* A_1 = (|A_0|^2 + |A_1|^2) s_0 + A_0^* n_0 + A_1 n_1^*, \quad (5)$$

$$\tilde{s}_1 = r_0 A_1^* - r_1^* A_0 = (|A_0|^2 + |A_1|^2) s_1 - A_0 n_1^* + A_1^* n_0. \quad (6)$$

Then, \tilde{s}_0 and \tilde{s}_1 will be passed to the maximum likelihood (ML) detector to estimate s_0 and s_1 . Considering the symmetry of s_0 and s_1 , the instantaneous received SNR per symbol can be obtained as

$$\gamma = \frac{(|A_0|^2 + |A_1|^2) E_s}{N_0}. \quad (7)$$

Considering $h_i \sim \mathcal{CN}(0, 1)$, we obtain A_0 and $A_1 \sim \mathcal{CN}(0, P_L \frac{N}{2})$. Consequently, γ becomes a central chi-square distributed random variable with four degrees of freedom with the following MGF [19]:

$$M_\gamma(s) = \left(\frac{1}{1 - \frac{s P_L N E_s}{2 N_0}} \right)^2. \quad (8)$$

From (8), the average symbol error probability (SEP) for M -PSK signaling can be obtained as [20]

$$P_e = \frac{1}{\pi} \int_0^{(M-1)\pi/M} \left(\frac{1}{1 + \left(\frac{\sin(\pi/M)^2}{\sin(\eta)^2} \right) \frac{P_L N E_s}{2 N_0}} \right)^2 d\eta \quad (9)$$

which can be simplified for BPSK as

$$P_e = \frac{1}{\pi} \int_0^{\pi/2} \left(\frac{1}{1 + \frac{P_L N E_s}{2 N_0 \sin(\eta)^2}} \right)^2 d\eta. \quad (10)$$

From (9), we observe that a transmit diversity of order two is still achieved by this scheme due to the fact that the RIS mimics a similar transmission methodology to the Alamouti's scheme over two time slots and preserves its orthogonality. Furthermore, the transmitted symbols have an SNR amplification achieved by the combination of the signals reflected from the RIS, where the SNR is enhanced by a factor of N , as seen from (10).

III. RIS-ASSISTED AND IM-BASED VBLAST SYSTEM: THE SIGNAL MODEL

The proposed RIS-assisted and IM-based VBLAST scheme utilizes the RIS in two different ways, first to eliminate the channel phases and compensate for fading, second to perform IM at both the transmitter and receiver side. This means that the proposed scheme benefits from the RIS in an effective way. Consequently, with the help of the RIS, the proposed scheme provides a significant BER performance enhancement and an effective boost in the spectral efficiency compared to the classical VBLAST scheme. The proposed scheme is shown in Fig. 2, where an $N_t \times N_r$ VBLAST system is being operated along with an RIS with N reflecting elements. Here, we assume a feedback link between S and the RIS to convey IM information to the RIS. The RIS-assisted and IM-based VBLAST scheme can be operated in three different modes namely, i) full IM mode, ii) partial-IM mode, and iii) enhancing mode. In what follows, we describe these three operating modes.

In the full-IM mode, at the transmitter side, the IM-based mapping and transmission can be described as follows. The

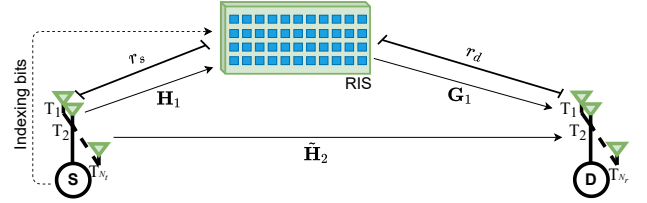


Fig. 2. RIS-assisted and IM-based $N_t \times N_r$ VBLAST scheme.

incoming bits will be divided into two groups, where the first group of $N_t \log_2 M$ bits will be used to select N_t independent M -QAM symbols to be transmitted from the available N_t transmitting antennas. The second group of $\log_2(N_t N_r)$ bits will be used by the RIS to select the indices of transmit and receive antenna, shown by l^* and m^* , corresponding to a $T_{l^*} - R_{m^*}$ pair of antennas, where the channel phases between them will be eliminated. This means that all possible combinations ($N_t N_r$) of the transmit-receive antenna indices will be used to convey IM bits, assuming $N_t N_r$ is an integer power of two. The overall spectral efficiency of the system becomes $N_t \log_2 M + \log_2(N_t N_r)$ bits per channel use (bpcu).

In the partial-IM mode, assuming that the same number of antennas is used at the transmitter and receiver side, the indices of the targeted antenna pair will be identical, $T_{l^*} - R_{l^*}$, where only $\log_2 N_t$ possible combinations will be used to convey the IM bits. The resulting spectral efficiency under this mode will be $N_t \log_2 M + \log_2 N_t$ bpcu, where the motivation here is to sacrifice spectral efficiency gained by IM in order to further enhance the BER performance through increasing the reliability of IM bits.

Finally, in the enhancing mode, IM is not performed at all and therefore, there is no need for a feedback link between S and D, instead, a fixed and predefined antenna pair will always be targeted by the RIS for the elimination of channel phases. Consequently, the best BER performance is achieved while preserving the same spectral efficiency for classical VBLAST, $N_t \log_2 M$. For all operating modes, we assume that perfect CSI is available at the both RIS and receiver side, which is a challenging but a reasonable assumption [10], [12]. We describe our scheme with an example.

Example: A 4×4 RIS-assisted VBLAST system operated in the full-IM mode with QPSK modulation transmits the bitstream of [00 01 10 11 00 01] as follows. The first 8 bits are modulated to 4 QPSK symbols and transmitted, in parallel, from the available 4 transmit antennas. The remaining 4 bits are used by the RIS to select the pair $T_1 - R_2$, since we implement the following mapping rule: 00 \rightarrow 1 and 01 \rightarrow 2. The RIS adjusts the reflection phases to eliminate the channel phases between T_1 and R_2 . On the other hand, the receiver tries to first estimate the indices of the selected antennas, and then successively detects the N_t independent M -QAM symbols.

For an $N_t \times N_r$ VBLAST system assisted by an RIS with N reflectors, the vector of the received signals $\mathbf{r} \in \mathbb{C}^{N_r \times 1}$ can be written as

$$\mathbf{r} = \left[\sqrt{P_{L1}} \mathbf{G}_1^T \Theta \mathbf{H}_1 + \sqrt{P_{L2}} \tilde{\mathbf{H}}_2 \right] \mathbf{x} + \mathbf{n} = \mathbf{V} \mathbf{x} + \mathbf{n} \quad (11)$$

where $\mathbf{H}_1 \in \mathbb{C}^{N \times N_t}$, $\mathbf{G}_1 \in \mathbb{C}^{N \times N_r}$ are the S-RIS and RIS-

D, uncorrelated Rician fading channel matrices, respectively. The S-D channel matrix $\tilde{\mathbf{H}}_2 \in \mathbb{C}^{N_r \times N_t}$ is a random matrix where its elements are independent and identically distributed (i.i.d) complex Gaussian random variables (RVs) with zero mean and unit variance, $\sim \mathcal{CN}(0, 1)$. K is the Rician factor standing for the ratio of LOS and NLOS power and $\Theta = \text{diag}([e^{j\Phi_1} e^{j\Phi_1} \dots e^{j\Phi_N}])$ is the matrix of RIS reflection phases. $\mathbf{x} \in \mathbb{C}^{N_t \times 1}$ is the vector of transmitted M -QAM symbols, $\mathbf{V} \in \mathbb{C}^{N_r \times N_t}$ is the S-RIS-D and S-D equivalent channel matrix and $\mathbf{n} \in \mathbb{C}^{N_r \times 1}$ is the vector of AWGN noise samples. P_{L1} and P_{L2} are the total path losses for S-RIS-D and S-D transmission paths, respectively, and more details are given in Section IV. The received signal by the m^{th} receiving antenna (R_m) can be represented as

$$r_m = \left[\sqrt{P_{L1}} \mathbf{g}_m^T \Theta \mathbf{H} + \mathbf{h}_2 \right] \mathbf{x} + n_m \quad (12)$$

where $\mathbf{h}_2 = \sqrt{P_{L2}} \tilde{\mathbf{h}}_2$ and $\tilde{\mathbf{h}}_2 \in \mathbb{C}^{1 \times N_t}$ is the S-D channel vector for the m^{th} receiving antenna. $\mathbf{g}_m \in \mathbb{C}^{N \times 1}$ is the RIS-D channel vector for the m^{th} receiving antenna, and n_m is the AWGN sample with $n_m \sim \mathcal{CN}(0, N_0)$. Expanding (12), we have

$$r_m = \sqrt{P_{L1}} \sum_{l=1}^{N_t} \left[\sum_{i=1}^N h_i^{(l)} e^{j\Phi_i} g_i^{(m)} \right] x^{(l)} + \mathbf{h}_2 \mathbf{x} + n_m \quad (13)$$

where $h_i^{(l)} = \alpha_i^l e^{-j\theta_i^{(l)}}$ is the S (l^{th} transmitting antenna)-RIS (i^{th} element) channel coefficient and $g_i^{(m)} = \beta_i^m e^{-j\psi_i^{(m)}}$ is RIS (i^{th} element)-D (m^{th} receiving antenna) channel coefficient. In this way, in order to eliminate the phases of the S-RIS-D channel between the antenna pair $T_{l^*} - R_{m^*}$, elements' phases of the RIS are adjusted as $\Phi_i = \theta_i^{(l^*)} + \Psi_i^{(m^*)}$, and (13) can be re-expressed for the $(m^*)^{\text{th}}$ receive antenna as

$$r_{m^*} = \sqrt{P_{L1}} \left[\sum_{i=1}^N \alpha_i^{l^*} \beta_i^{m^*} \right] x^{(l^*)} + \sum_{l=1, l \neq l^*}^{N_t-1} \left[\sum_{i=1}^N h_i^{(l)} e^{j\Phi_i} g_i^{(m^*)} \right] x^{(l)} + \mathbf{h}_2 \mathbf{x} + n_{m^*}. \quad (14)$$

(14) can be interpreted as follows. The first term illustrates the amplification gained by the constructive combining of the signals reflected from the RIS and belongs to the symbol $x^{(l^*)}$. This constructive combining will result in an SNR gain of N^2 for this symbol as in [5]. Hence, the BER performance of this symbol will be boosted up and consequently, it will be the strongest symbol where the nulling and canceling algorithm starts with. This also means that the error propagation from the first symbol to the remaining ones will be significantly mitigated and the overall BER performance will be improved. The second term shows the destructive interference of the signals reflected from the RIS, which belongs to the other symbols. Finally, the third term corresponds to the interference received by the $(m^*)^{\text{th}}$ receiving antenna through the S-D transmission path for all the transmitted symbols. Hence, compared to the classical VBLAST, an RIS will introduce N times extra interference for each received symbol. Nevertheless, assuming that the CSI over S-RIS-D is available at the receiver side, then this interference can be handled readily.

A. Detection Algorithms

At the receiver side, we introduce two novel nulling-based detectors to detect the transmit-receive antenna indices targeted by the RIS for channel phases elimination. According to Algorithm 1, the optimal detector performs an exhaustive search for l^* and m^* jointly, as follows. For each iteration, the detector determines $\Theta^{(l,m)}$ and then constructs $\hat{\mathbf{V}}^{(l,m)}$. Next, the nulling-based procedure will be used to detect the first symbol, which has the highest SNR, assumed to be transmitted and received by the antenna pair $T_l - R_m$. Finally, the pair l and m associated with the symbol that has the minimum squared Euclidean distance will be picked as the pair l^* and m^* .

In Algorithm 1, $\hat{\mathbf{V}}^{(l,m)}$ is the index-estimated S-RIS-D and S-D equivalent channel matrix assuming the antenna pair $T_l - R_m$ was targeted by the RIS for channel phases elimination. $\Theta^{(l,m)}$ is the diagonal RIS phases matrix where its i^{th} element $\Phi_i = \theta_i^{(l)} + \Psi_i^{(m)}$ corresponds to the phase elimination for the S-RIS-D channel between T_l and R_m . $(\cdot)^+$ is Moore-Penrose pseudo-inverse operator, $(\hat{\mathbf{V}}^{(l,m)})^+ = \hat{\mathbf{V}}^{(l,m)\dagger} (\hat{\mathbf{V}}^{(l,m)} \hat{\mathbf{V}}^{(l,m)\dagger})^{-1}$, where $(\cdot)^\dagger$ is the Hermitian operator. $(\mathbf{W}^{(l,m)})_j$ is the j^{th} row of $\mathbf{W}^{(l,m)}$. k_l is the index of the row, which has the minimum squared Euclidean norm, of the matrix $\mathbf{W}^{(l,m)}$, corresponding to the symbol with the highest SNR. $(\mathbf{W}^{(l,m)})_{k_l}$ is the k_l^{th} row of $\mathbf{W}^{(l,m)}$, y_{k_l} is the k_l^{th} symbol after nulling the interference of the other symbols. $\mathcal{Q}(\cdot)$ returns the squared Euclidean distance, $D_{l,m}$, of the closest M -QAM symbol associated with y_{k_l} . Hence, $\hat{\mathbf{V}}^{(\hat{l}, \hat{m})}$ associated with the minimum distance $D_{\hat{l}, \hat{m}}$ is the most likely the equivalent channel matrix that corresponds to the current adjustment of the RIS phases. By estimating l^* and m^* , the IM bits conveyed by the adjustment of the RIS phases will be obtained. In order to reduce the complexity of

Algorithm 1 Optimal detector: Detecting the antenna indices l^* and m^* jointly.

Require: $\mathbf{H}_1, \tilde{\mathbf{H}}_2, \mathbf{G}_1, \mathbf{r}, \sqrt{P_{L1}}, \sqrt{P_{L2}}$

- 1: **for** $l = 1 : N_t$ **do**
- 2: **for** $m = 1 : N_r$ **do**
- 3: $\hat{\mathbf{V}}^{(l,m)} = \sqrt{P_{L1}} \mathbf{G}_1^T \Theta^{(l,m)} \mathbf{H}_1 + \sqrt{P_{L2}} \tilde{\mathbf{H}}_2$
- 4: $\mathbf{W}^{(l,m)} = (\hat{\mathbf{V}}^{(l,m)})^+$
- 5: $k_l = \arg \min_{j \in \{1, 2, \dots, N_t\}} \|(\mathbf{W}^{(l,m)})_j\|^2$ {Ordering}
- 6: $\mathbf{s}_{k_l} = (\mathbf{W}^{(l,m)})_{k_l}$
- 7: $y_{k_l} = \mathbf{s}_{k_l}^T \mathbf{r}$ {Nulling}
- 8: $D_{l,m} = \mathcal{Q}(y_{k_l})$
- 9: **end for**
- 10: **end for**
- 11:

$$\{\hat{l}, \hat{m}\} = \arg \min_{\substack{l \in \{1, 2, \dots, N_t\} \\ m \in \{1, 2, \dots, N_r\}}} D_{l,m}$$

$$12: \quad \hat{\mathbf{V}} = \sqrt{P_{L1}} \mathbf{G}_1^T \Theta^{(\hat{l}, \hat{m})} \mathbf{H}_1 + \sqrt{P_{L2}} \tilde{\mathbf{H}}_2$$

13: **return** $\hat{\mathbf{V}}$

the detector proposed in Algorithm 1, the receiving antenna index, m^* , can be detected using a greedy detector instead of the joint exhaustive search for l^* and m^* . In this way, m^* can be detected by finding the receiving antenna with the highest instantaneous energy:

$$\hat{m} = \arg \max_{m \in \{1, 2, \dots, N_r\}} |r_m|^2 \quad (15)$$

Next, a nulling-based procedure is used to search for l^* while fixing \hat{m} found from (15). This detector is represented as a sub-optimal one and Algorithm 2 illustrates its detection steps.

After obtaining the S-RIS-D and S-D equivalent channel matrix, $\hat{\mathbf{V}}$, it will be used by Algorithm 3 to detect the N_t independent symbols as in the case of classical VBLAST [17]. In Algorithm 3, $\tilde{\mathcal{Q}}(\cdot)$ is the slicing function, $(\hat{\mathbf{V}})_{k_i}$ is the k_i^{th} column of $\hat{\mathbf{V}}$ and $(\hat{\mathbf{V}}_{k_i}^+)^+$ is pseudo inverse of the matrix obtained by zeroing the columns of $\hat{\mathbf{V}}$ with indices k_1, k_2, \dots, k_i . Finally, \mathbf{r}_{i+1} is the signal vector after subtracting the interference contribution of the previously detected symbol $\hat{\mathbf{x}}_{k_i}$.

Algorithm 2 Sub-optimal detector: Detecting the antenna indices l^* and m^* sequentially.

Require: $\mathbf{H}_1, \tilde{\mathbf{H}}_2, \mathbf{G}_1, \mathbf{r}, \sqrt{P_{L1}}, \sqrt{P_{L2}}$

1:

$$\hat{m} = \arg \max_{m \in \{1, 2, \dots, N_r\}} |r_m|^2$$

2: **for** $l = 1 : N_t$ **do**

$$3: \quad \hat{\mathbf{V}}^{(l, \hat{m})} = \sqrt{P_{L1}} \mathbf{G}_1^T \Theta^{(l, \hat{m})} \mathbf{H}_1 + \sqrt{P_{L2}} \tilde{\mathbf{H}}_2$$

$$4: \quad \mathbf{W}^{(l, \hat{m})} = (\hat{\mathbf{V}}^{(l, \hat{m})})^+$$

$$5: \quad k_l = \arg \min_{j \in \{1, 2, \dots, N_t\}} |(\mathbf{W}^{(l, \hat{m})})_j|^2 \quad \{\text{Ordering}\}$$

$$6: \quad \mathbf{s}_{k_l} = (\mathbf{W}^{(l, \hat{m})})_{k_l}$$

$$7: \quad y_{k_l} = \mathbf{s}_{k_l}^T \mathbf{r} \quad \{\text{Nulling}\}$$

$$8: \quad D_l = \mathcal{Q}(y_{k_l})$$

9: **end for**

10:

$$\hat{l} = \arg \min_{l \in \{1, 2, \dots, N_t\}} D_l$$

$$11: \quad \hat{\mathbf{V}} = \sqrt{P_{L1}} \mathbf{G}_1^T \Theta^{(\hat{l}, \hat{m})} \mathbf{H}_1 + \sqrt{P_{L2}} \tilde{\mathbf{H}}_2$$

12: **return** $\hat{\mathbf{V}}$

B. Computational Complexity Analysis

At the receiver side, first, the RIS-assisted VBLAST scheme uses Algorithm 1 or Algorithm 2 to detect the indices l^* and m^* . Second, the receiver uses Algorithm 3 to detect the N_t transmitted M -QAM symbols. Here, we calculate the computational complexity associated with Algorithms 1, 2, and 3.

Denoting the total number of complex multiplications (CMs) required by Algorithms 1, 2, and 3 as C_1 , C_2 , and C_3 , respectively, then from Table 1, C_1 , C_2 and C_3 can be calculated as follows

Algorithm 3 ZF-based successive nulling and canceling to detect the transmitted M -QAM symbols.

Require: $\hat{\mathbf{V}}, \mathbf{r}$

$$\mathbf{r}_1 = \mathbf{r}$$

$$\mathbf{W}_1 = \hat{\mathbf{V}}^+$$

$$k_1 = \arg \min_{j \in \{1, 2, \dots, N_t\}} |(\mathbf{W}_1)_j|^2$$

for $i = 1 : N_t - 1$ **do**

$$\mathbf{s}_{k_i} = (\mathbf{W}_i)_{k_i}$$

$$y_{k_i} = \mathbf{s}_{k_i}^T \mathbf{r}_i$$

$$\hat{x}_{k_i} = \mathcal{Q}(y_{k_i}) \quad \{\text{Slicing}\}$$

$$\mathbf{r}_{i+1} = \mathbf{r}_i - \hat{x}_{k_i} (\hat{\mathbf{V}})_{k_i} \quad \{\text{Canceling}\}$$

$$\mathbf{W}_{i+1} = (\hat{\mathbf{V}}_{k_i}^+)^+$$

$$k_{i+1} = \arg \min_{j \in \{1, \dots, N_t\} \setminus \{k_1, \dots, k_i\}} |(\mathbf{W}_{i+1})_j|^2$$

end for

$$\mathbf{s}_{k_{i+1}} = (\mathbf{W}_{i+1})_{k_{i+1}}$$

$$y_{k_{i+1}} = \mathbf{s}_{k_{i+1}}^T \mathbf{r}_{i+1}$$

$$\hat{x}_{k_{i+1}} = \mathcal{Q}(y_{k_{i+1}})$$

return $\hat{\mathbf{x}}$

$$C_1 = N_t N_r [(N_r N + N_r N N_t) + (2N_r^2 N_t + N_r^3) + N_t N_r + N_r + 2^M], \quad (16)$$

$$C_2 = N_r + N_t [(N_r N + N_r N N_t) + (2N_r^2 N_t + N_r^3) + N_t N_r + N_r + 2^M]. \quad (17)$$

$$C_3 = (2N_r^2 N_t + N_r^3) + N_t N_r + (N_t - 1)[N_r + 2^M + N_r + (2N_r^2 N_t + N_r^3) + N_t N_r] + N_r + 2^M. \quad (18)$$

In order to provide a useful insight on the overall complexity, let $N_t = N_r$. Then (16), (17), and (18) can be rewritten as

$$C_1 = N(N_r^3 + N_r^4) + 3N_r^5 + N_r^4 + N_r^3 + N_r^2 2^M, \quad (19)$$

$$C_2 = N_r + N(N_r^2 + N_r^3) + 3N_r^4 + N_r^3 + N_r^2 + N_r 2^M, \quad (20)$$

$$C_3 = 4N_r^3 + 3N_r^2 + N_r 2^M + 3N_r^4 + N_r + 2^M. \quad (21)$$

From (16) and (17), it can be seen that the number of antennas and the number of RIS reflecting elements both have a significant contribution to the computational complexity of detecting the antenna indices l^* and m^* . This is still valid even if we consider the fact that N is, practically, much larger than N_r , since the latter still has a higher exponent. From (19) and (20), the overall computational complexity level can be obtained as $\sim \mathcal{O}(N(N_r^3 + N_r^4) + N_r^5)$, and $\sim \mathcal{O}(N(N_r^2 + N_r^3) + N_r^4)$, for Algorithms 1 and 2, respectively. Comparing both algorithms, we observe that the overall computational complexity is dominated by that of constructing $\hat{\mathbf{V}}^{(l, m)}$. Compared to the classical VBLAST scheme, where the receiver computational complexity will be equivalent to that of Algorithm 3 only, $\sim \mathcal{O}(N_r^4)$, RIS-assisted IM-based VBLAST scheme has an extra complexity of $\sim \mathcal{O}(N(N_r^3 + N_r^4))$ and $\sim \mathcal{O}(N(N_r^2 + N_r^3))$ for Algorithms 1 and 2, respectively. The cost of this additional complexity stems from the construction of $\hat{\mathbf{V}}^{(l, m)}$, which is required to detect the transmitted symbols and the indices of the targeted transmit-receiving antennas. In a brief, C_1 or C_2 is the additional computational complexity that is required to operate a classical VBLAST system as an RIS-assisted system.

TABLE I
COMPUTATIONAL COMPLEXITY DERIVATION STEPS OF NULLING-BASED
DETECTION ALGORITHMS.

Operation	CMs
Searching for \hat{m}	N_r
Constructing $\hat{\mathbf{V}}^{(l,m)}$	$N_r N + N_r N N_t$
Pseudo inverse of $\hat{\mathbf{V}}^{(l,m)}$	$2N_r^2 N_t + N_r^3$
Ordering	$N_t N_r$
Nulling	N_r
Getting $D_{l,m}$	2^M

IV. SIMULATION RESULTS

In this section, exhaustive computer simulations are provided for the proposed schemes against their counterparts. We consider realistic setups and path loss models where both transmitter and receiver located in an indoor environment and Fig. 3 shows the block diagrams of the benchmark schemes. In all simulations, the SNR is defined to be E_s/N_0 .

Figs. 3 (a) and (c) show the system setups for the classical Alamouti and VBLAST schemes, where the S-D channel is assumed to follow a Rayleigh fading (i.e., consist of a non-LOS link). For the RIS-AP scheme shown in Fig. 3 (b), the S-D transmission path is assumed to be fully blocked by obstacles and the only transmission path is through the RIS, where the S-RIS path is LOS dominated and the RIS-D path follow Rayleigh fading [5].

For classical VBLAST and Alamouti schemes, where there is no RIS, the path loss is calculated for an operating frequency of 1.8 GHz, as follows [21]

$$P_L^{(S-D)}(R)[\text{dB}] = 42.7 + 20 \log_{10} R + 13.8 \quad (22)$$

where R is the S-D separation distance, 42.7 dB is the path loss at one meter distance, and 13.8 dB corresponds to the path loss of two walls each having 6.9 dB of path loss.

For the RIS-assisted Alamouti and RIS-AP schemes, the S-RIS-D path loss, P_L , is calculated as follows [22]

$$P_L^{(S-RIS-D)} = \frac{\lambda^4}{256\pi^2 r_s^2 r_d^2} \quad (23)$$

where λ is the wavelength of the operating frequency (1.8 GHz). Finally, for RIS-assisted and IM-based VBLAST scheme, P_{L2} and P_{L1} are calculated from (22) and (23), respectively. For RIS-assisted Alamouti, RIS-AP, and classical Alamouti's schemes we have $r_s = 1$ m, $r_d = 9$ m, $b = 0.5$ m, and $R = 9.85$ m. On the other hand, for RIS-assisted and IM-based VBLAST and classical VBLAST schemes, we have $r_s = 3$ m, $r_d = 3$ m, $b = 0.5$ m, and $R = 5.91$ m.

Fig. 4 illustrates the BER performance of the RIS-assisted Alamouti's scheme versus the classical Alamouti's scheme for a 2×1 MISO system and the blind case of RIS-AP in [5]. We observe that a second order transmit diversity is achieved using a single RF signal generator thanks to the RIS. In addition, an SNR gain is also achieved with a factor of N . As it can be seen, a BER performance gain of 10 dB can be achieved by using 64 RIS elements, then, the performance improvement continues linearly as N increases, where doubling N results in a 3 dB performance gain, which can be verified from (10).

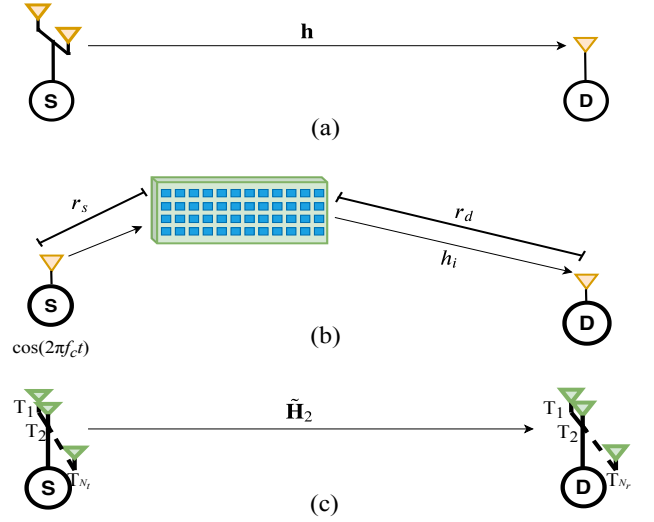


Fig. 3. (a) Classical Alamouti's scheme. (b) RIS-AP scheme. (c) Classical VBLAST scheme.

Hence, the RIS-assisted Alamouti's scheme outperforms the classical Alamouti's scheme in terms of the BER performance and the required RF resources on the transmitter side. Also, compared to the blind scheme of RIS-AP in [5], we see that the proposed scheme clearly shines out by a diversity of order two due to the orthogonality of Alamouti's transmission matrix.

For the RIS-assisted and IM-based VBLAST scheme, we considered the existence and absence of a LOS component for the S-RIS, and RIS-D channels. Therefore, the simulations are performed with $K = 5$, and $-\infty$ dB, where K values can change dramatically within the same indoor environment depending on the location of the transmitter and receiver [23].

In Figs. 5 and 6, we compare RIS-assisted and IM-based VBLAST with classical VBLAST for 2×2 MIMO setup. Here, the spectral efficiency of classical VBLAST is 2 b/s/Hz, while it is 3 and 4 b/s/Hz for the RIS-assisted and IM-based VBLAST, in partial and full-IM modes, respectively, with BPSK. Thus, the spectral efficiency for the RIS-assisted IM-based VBLAST is significantly boosted compared to the classical VBLAST due to the extra IM bits conveyed by our antenna pair selection methodology.

In Fig. 5 we compare the BER performance of RIS-assisted and IM-based VBLAST scheme, under the Rayleigh fading assumption for the S-RIS-D transmission path, with classical VBLAST scheme. We observe that the proposed scheme operated in full-IM mode provides an improved BER at low to mid SNR values, while saturating to the BER performance of the classical VBLAST at high SNR. Nevertheless, compared to the classical VBLAST scheme, the spectral efficiency is doubled for the proposed scheme. Furthermore, the sub-optimal detector shows the same BER performance as for the optimal one, which means that the detection process can be simpler in terms of the complexity level. It can be also seen that using discrete phase shifts (only four different phase shifts) for the RIS elements, as considered in [24], and [25], achieves almost the same performance for the continuous phase shifts adjustment. This shows that the RIS design can be simplified to control each element through 2-bits only.

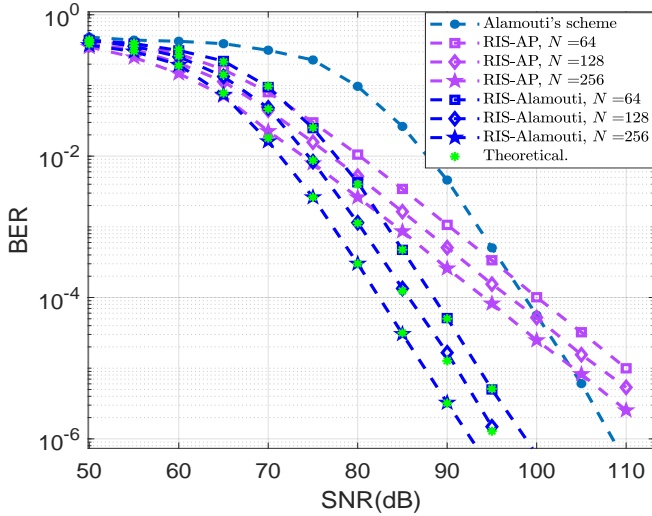


Fig. 4. BER performance of RIS-assisted Alamoutis scheme versus 2×1 classical Alamoutis scheme and RIS-AP (Blind) scheme, with different N values and BPSK.

Furthermore, the partial-IM and enhancing modes show a significant BER performance gain of 16 and 28 dB, respectively, compared to the classical VBLAST scheme. It is worth noting that, the partial-IM scheme increases the spectral efficiency by 50%.

In Fig. 6, the BER performance curves are shown for the RIS-assisted and IM-based VBLAST scheme considering the existence of LOS component ($K = 5$ dB) between S and the RIS, and between the RIS and D. Compared to the classical VBLAST scheme, the impact of the LOS component on the RIS performance can be clearly seen for the proposed scheme. The full-IM and partial-IM modes need an SNR increase of 5-10 dB in order to increase the spectral efficiency by 2 and 1.5 fold, respectively. This can be explained by the lack of diversity due to the LOS component in the S-RIS and RIS-D channels. Therefore, the receiver makes more errors while detecting the targeted antenna indices, l^* and m^* . Since the construction of $\hat{\mathbf{V}}$ depends on l^* and m^* , the erroneous detection of them reflects on the detection of the M -QAM symbols. Furthermore, it can be noted that the sub-optimal (greedy) detector provides an error floor even with an RIS of 512 elements. This is, also, due to the LOS component, which makes the difference in the instantaneous energy, received by all the receiving antennas, trivial. Nevertheless, the enhancing mode still provides a BER performance gain of 4 dB compared to the classical VBLAST scheme.

Considering different operating modes, from Fig. 5 and 6, it can be seen that the best BER performance can be achieved with the enhancing mode where there is no IM and the RIS amplification gain is directed towards a fixed and predefined antenna pair. Also, according to the K value, the proposed scheme has the flexibility to operate in one of the previously mentioned modes in order to increase the spectral efficiency and/or enhance the BER performance.

Finally, it is worth noting that, from (22) and (23), comparing the S-RIS-D and S-D communication links, we obtain 7.86 dB additional path loss, under the given separation distances,

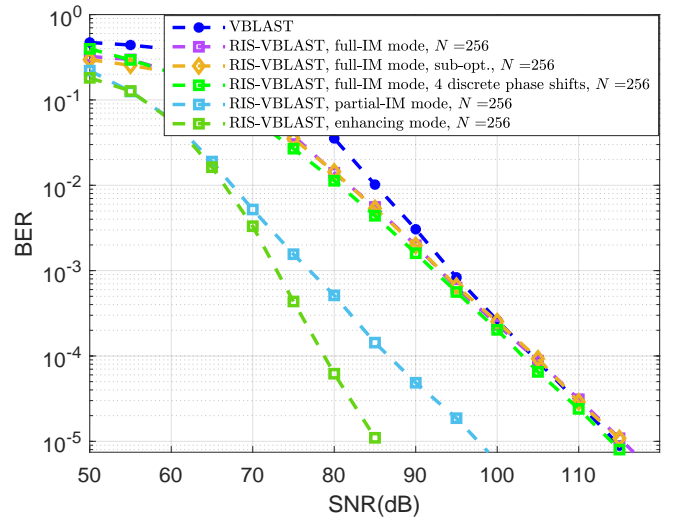


Fig. 5. BER performance of RIS-assisted and IM-based VBLAST scheme versus classical VBLAST with 2×2 MIMO setup, BPSK, and $K = -\infty$ dB.

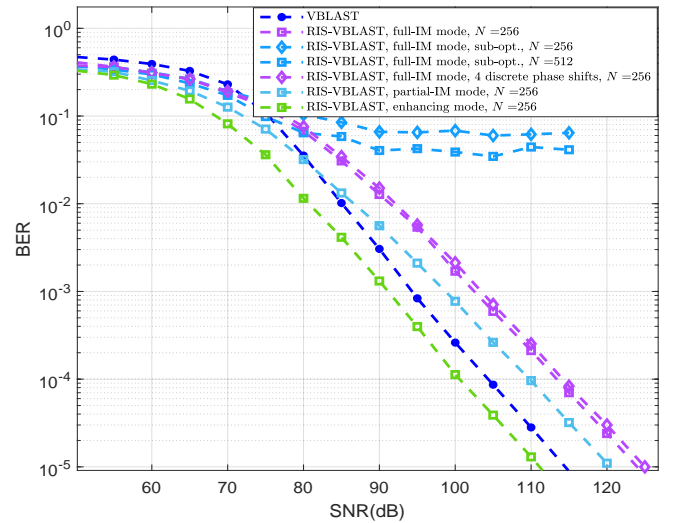


Fig. 6. BER performance of RIS-assisted and IM-based VBLAST scheme versus classical VBLAST with 2×2 MIMO setup, BPSK, and $K = 5$ dB.

for RIS-AP and RIS-assisted Alamouti schemes compared to the classical Alamouti's scheme. In the same way, for RIS-assisted and IM-based VBLAST scheme, where there are two communication links, there is an additional path loss of 12.29 dB for the S-RIS-D compared to the S-D communication link. This shows that the transmission over the RIS has considerably higher path loss compared to the direct transmission without RIS. Nevertheless, the additional path loss can be compensated by choosing the proper RIS size [22], [26], as we showed in our proposed schemes.

V. CONCLUSION

In this paper, we have proposed novel designs for MIMO systems with the assistance of RISs. Although only VBLAST and Alamouti's schemes have been considered in this study, our concepts can be applied for other MIMO schemes as well. Applying the considered concept to space-time codes in large scale MIMO setups with a large number of antennas may

show the remarkable advantage for this scheme by utilizing a single RF signal generator instead of multiple RF chains. Furthermore, RIS-assisted Alamouti's scheme is capable of achieving an N times SNR enhancement in addition to a transmit diversity order of two and the RIS-assisted IM-based VBLAST scheme is able to provide a significant BER performance gain in addition to the noticeable increasing in the spectral efficiency by the smart methodology of channel phases elimination. Considering the simplicity of implementation and deployment, both schemes do not require a significant reconfiguration for the existing MIMO setups, particularly in their receiver architectures, which makes them practical and feasible alternatives for future wireless systems.

REFERENCES

- [1] E. Basar, M. Di Renzo, J. de Rosny, M. Debbah, M.-S. Alouini, and R. Zhang, "Wireless communications through reconfigurable intelligent surfaces," *IEEE Access*, vol. 7, pp. 116753 - 116773, Sep. 2019.
- [2] Q. Wu, R. Zhang, "Towards smart and reconfigurable environment: intelligent reflecting surface aided wireless network," *IEEE Commun. Mag.*, vol. 58, pp. 106 - 112, Nov. 2019.
- [3] S. Gong *et al.*, "Towards smart radio environment for wireless communications via intelligent reflecting surfaces: A comprehensive survey," Dec. 2019. [Online]. Available: arXiv:1912.07794.
- [4] J. Zhao, "A survey of intelligent reflecting surfaces (irss): Towards 6g wireless communication networks," Jul. 2019. [Online]. Available: arXiv:1907.04789.
- [5] E. Basar, "Transmission through reconfigurable intelligent surfaces: A new frontier in wireless communications," in *Proc. European Conf. Netw. Commun. (EuCNC 2019)*, Valencia, Spain, June 2019. [Online]. Available: arXiv:1902.08463v2.
- [6] —, "Reconfigurable intelligent surface-based index modulation: A new beyond MIMO paradigm for 6G," *IEEE Trans. Comm.(to appear)*. Feb. 2020. [Online]. Available: arXiv:1904.06704.
- [7] X. Tan, Z. Sun, J. M. Jornet, and D. Pados, "Increasing indoor spectrum sharing capacity using smart reflect-array," in *Proc. 2016 IEEE Int. Conf. Commun. (ICC)*, Kuala Lumpur, Malaysia, May 2016, pp. 1–6.
- [8] C. Huang, G. C. Alexandropoulos, A. Zappone, M. Debbah, and C. Yuen, "Energy efficient multi-user MISO communication using low resolution large intelligent surfaces," in *Proc. IEEE Global Commun. Conf.*, Abu Dhabi, UAE, Dec. 2018.
- [9] Q. Wu and R. Zhang, "Intelligent reflecting surface enhanced wireless network: Joint active and passive beamforming design," in *Proc. IEEE Global Commun. Conf.*, Abu Dhabi, UAE, Dec. 2018. [Online]. Available: arXiv:1809.01423.
- [10] —, "Intelligent reflecting surface enhanced wireless network: Joint active and passive beamforming," *IEEE Trans. Wireless Commun.*, June 2019. [Online]. Available: arXiv:1810.03961v2.
- [11] X. Yu, D. Xu, and R. Schober, "MISO wireless communication systems via intelligent reflecting surfaces," in *Proc. 2019 IEEE/CIC Int. Conf. Commun. (ICCC)*, Changchun, China, Aug. 2019. [Online]. Available: arXiv:1904.12199.
- [12] Q.-U.-A. Nadeem, A. Kammoun, A. Chaaban, M. Debbah, and M.-S. Alouini, "Asymptotic max-min SINR analysis of reconfigurable intelligent surface assisted MISO systems," Mar. 2019. [Online]. Available: arXiv:1903.08127.
- [13] . zdogan, E. Bjrnson, E. G. Larsson, "Using intelligent reflecting surfaces for rank improvement in MIMO communications," Feb. 2020. [Online]. Available: arXiv:2002.02182.
- [14] S. Zhang, R. Zhang, "Capacity characterization for intelligent reflecting surface aided mimo communication," Oct. 2019. [Online]. Available: arXiv:1910.01573.
- [15] W. Jiang., Y. Zhang, J. Wu, W. Feng, Y. Jin, "Intelligent reflecting surface assisted secure wireless communications with multiple-transmit and multiple-receive antennas," Jan. 2020. [Online]. Available: arXiv:2001.08963.
- [16] J. Chen, Y.-C Liang, H. V. Cheng, W. Yu, "Channel estimation for reconfigurable intelligent surface aided multi-user mimo systems," Dec. 2019 [Online]. Available: arXiv: 1912.03619.
- [17] P.W. Wolniansky, G.J. Fosni, G.D. Golden, R.A. Valenzuela, "V-BLAST: An architecture for realizing very high data rates over the rich-scattering wireless channel," 1998 URSI International Symposium on Signal, System and Electronics, Pisa, Italy, pp. 295-300, Sep. Oct 1998.
- [18] S. Alamouti, "A simple transmit diversity technique for wireless communications," *IEEE J. Sel. Areas Commun.*, vol. 16, no. 8, pp. 1451-1458, Oct. 1998.
- [19] J. G. Proakis, *Digital Communication*. 5th ed. New York: McGrawHill, 2008.
- [20] M. Simon, M. S. Alaoui, *Digital Communications over Fading Channels*. 2nd ed. New Jersey: John Wiley and Sons, 2005.
- [21] E. Damosso, L. M. Coreia, *COST Action 231: Digital Mobile Radio Towards Future Generation Systems: Final Report*, 1999.
- [22] S.W. Ellingson, "Path loss in reconfigurable intelligent surface-enabled channels," Dec. 2019. [Online]. Available: arXiv:1912.06759v1.
- [23] C.H.Y. Eugene, K. Sakaguchi , K. Araki, "Experimental and analytical investigation of MIMO channel capacity in an indoor line-of-sight (LOS) environment," *IEEE 15th International Symposium on Personal, Indoor and Mobile Radio Communications (IEEE Cat. No.04TH8754)*, Barcelona, Spain, Sep. 2004.
- [24] H. Zhang, B. Di, L. Song, Z. Han, "Reconfigurable intelligent surfaces assisted communications with limited phase shifts: How many phase shifts are enough?" *IEEE Trans. Veh. Technol. (to appear)*. Feb. 2020. [Online]. Available: arXiv:1912.01477.
- [25] Q. Wu R. Zhang, "Beamforming optimization for intelligent reflecting surface with discrete phase shifts," *ICASSP 2019 - 2019 IEEE International Conference on Acoustics, Speech and Signal Processing (ICASSP)*, Brighton, United Kingdom, May 2019.
- [26] W. Tang *et al.*, "Wireless communications with reconfigurable intelligent surface: Path loss modeling and experimental measurement," Nov. 2019. [Online]. Available: arXiv:1911.05326.